Additively Manufactured Aluminium Alloys

Metal additive manufacturing (MAM), also known as metal 3D printing, is a rapidly growing industry based on the fabrication of complex metal parts with improved functionalities. During MAM, metal parts are produced in a layer by layer fashion using 3D computer–aided design models. The advantages of using this technology includes the reduction of materials waste, high efficiency for small production runs, near net shape manufacturing, ease of change or revision of versions of a product, support of lattice structures, and rapid prototyping. Numerous metals and alloys can nowadays be processed by additive manufacturing techniques. Among them, Al-based alloys are of great interest for the automotive and aeronautic industry due to their relatively high strength and stiffness to weight ratio, good wear and corrosion resistance, and recycling potential. The special conditions associated with the MAM processes are known to produce in these materials a very fine microstructure with unique directional growth features far from equilibrium. This distinctive microstructure, together with other special features and microstructural defects originating from the additive manufacturing process are known to greatly influence the corrosion behavior of these materials. Several works have already been conducted in this direction. However, a number of issues concerning the corrosion and corrosion protection of these materials are still not well understood. This work reviews the main studies to date investigating the corrosion aspects of additively manufactured aluminium alloys. It also provides a summary and outlook of relevant directions to be explored in future research.

Keywords: Metal additive manufacturing ; aluminium alloys ; corrosion behavior ; microstructure ; corrosion protection

1. Introduction

Metal additive manufacturing (MAM), commonly known as metal 3D-printing, is a process by which complex multifunctional metal parts are produced in a layer by layer fashion using 3D computer-aided design (CAD) models [1][2][3][4][5][6]. Several MAM techniques are available. They can be separated into two main groups: direct energy deposition (DED) methods and powder bed fusion (PBF) technology [7]. During direct energy deposition, focused thermal energy is used to fuse materials by melting as they are being deposited; while during powder bed fusion, thermal energy selectively fuses regions of a powder bed [7]. DED processes such as wire arc additive manufacturing (WAAM) and laser metal deposition (LMD) can generally be used on existing parts of arbitrary geometry with a relatively high deposition rate; however, the shape complexity is limited. This makes DED processes the preferred methodology for repairing or improving existing parts [8]. On the other hand, on PBF methods such as selective laser melting (SLM), selective laser sintering (SLS), and electron beam melting (EBM), the dimension of the pieces is limited and the starting substrate has to be a flat surface. However, they generally allow the fabrication of pieces with extremely high structural complexity at a relatively high level of precision. Among the several MAM processes, those utilizing a metal powder feedstock and a laser source to achieve the metal fusion are the most widely used [1][2][3][4][5][6]. From those, SLM is regarded as the most used and studied MAM method. This is not only because it allows a higher level of precision compared to other MAM techniques, but also because (in contrast to SLS) it allows the full melting of the material, and therefore the production of solid and dense metal parts in a single process (without the need to use binders and/or other post-process furnace operations).

Additive manufacturing is considered one of the enabling technologies for Industry 4.0 [9]. In particular, MAM presented a global market valued at € 2.02 billion in 2019 [10]. This included systems, materials, and services. MAM allows the near-net shape manufacturing of geometrically complex parts such as lattice structures and 3D structures with undercuts or cavities, which is why this technology has found numerous applications in industries such as medical implants, energy, aerospace, and automotive. As an example in aerospace applications, MAM has made possible the re-design of complex fuel injector nozzles (commonly requiring the assembly of more than 20 parts) in a single operation [11][12], as well as the re-design of several other complex engineered parts, resulting in considerable cost and weight reduction. In aerospace, as well as in the automotive industry, MAM is also actively used in prototyping and the fabrication of custom tooling.
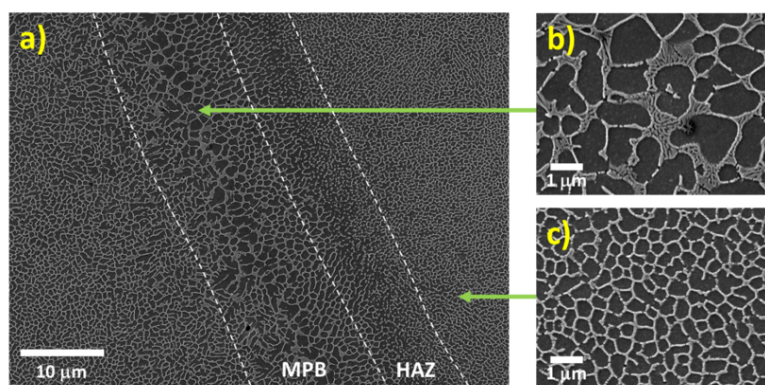
Nowadays, a great number of metals and alloys can be processed by additive manufacturing techniques, depending mainly on the availability of the raw materials as metal powders or metal wires [5]. Amongst these, aluminium alloys are of great interest for applications requiring high strength and stiffness to weight ratio, good wear and corrosion resistance, and recycling potential, which is why they are attracting increasing attention of the automotive and aerospace industries [12][13]. The most common Al-based alloys processed by additive manufacturing (AM) either for commercial use or for research purposes are [5][14][15]: AlSi12, AlSi10Mg, AlSi7Mg0.6, AlSi9Cu3, AlSi5Cu3Mg, AA1050, AA2017, AA2024, AA2219, AA6061, AA7020, AA7050, AA7075, and AA5083; next to proprietary industrial alloys like Scalmalloy. From those, Al-Si alloys, and more specifically AlSi10Mg (followed by AlSi12), are undoubtedly the most investigated and commercially used additively manufactured Al-based alloys. These materials, particularly relevant for light-weight and high-strength applications, are widely used for aluminium casting due to the proximity to the eutectic composition (~12.5% Si) [16]. Therefore, they are relatively easy to process by laser applications, which are known to lead to a small solidification range [17]. Additionally, minor additions of magnesium (0.3–0.5 wt.% Mg) are known to induce hardening of the alloy by forming Mg_2Si precipitates upon natural or artificial ageing treatments [18]. However, the actual formation of these precipitates on additively manufactured Al-Si parts is still a topic of discussion.

Due to the special conditions of the MAM processes (namely that the metal powder used is already pre-alloyed, and the melting occurs in small pools that rapidly solidify), a very fine microstructure with unique directional growth features far from equilibrium is achieved [1]. This distinctive microstructure, together with other special features and microstructural defects originating from the additive manufacturing process is known to greatly influence the corrosion behaviour of these materials. Sander et al. [19] and Kong et al. [20] reviewed the impact of these special features and defects on the corrosion performance of additively manufactured metals. These works also consider the main corrosion issues of several additively manufactured materials, including some studies on Al alloys. Zhang et al. [17] presented a review of Al-based alloys summarizing the microstructural characteristics and mechanical properties. Chen et al. [21] reviewed the main research studying the corrosion behaviour of selective laser melted Al alloys, classified/structured by the used technique.

2. Al-Si Alloys

2.1. Effect of Microstructure on Corrosion Behavior

Several studies characterizing the microstructure of as-built additively manufactured Al-Si alloys have been conducted in recent years [22][23][24][25][26][27][28][29][30][31][32]. As-built specimens exhibit a fine distribution of Si, forming a three-dimensional network that encloses the primary face-centred cubic α-Al in very small cells (see Figure 1). The size of these cells varies over the melt pool due to the thermal gradient created by the moving heat source. Finer cells are formed towards the middle of the melt pools (MP), while coarser cells are present in the melt pool borders (MPBs) [25]. A marked anisotropy has been described in past studies concerning the shape of these cells. These cells are known to present an approximately round shape in the plane parallel to the building platform (XY), whereas in the plane perpendicular to the building platform (XZ) more elongated cells have been observed [25][31]. A heat-affected zone (HAZ) located right outside the borders of the melt pools has also been identified (see Figure 1). This HAZ, in which the silicon network is partly broken and discontinuous, has been associated with overheating of the underlying layer during the scanning of a newly deposited layer [25].
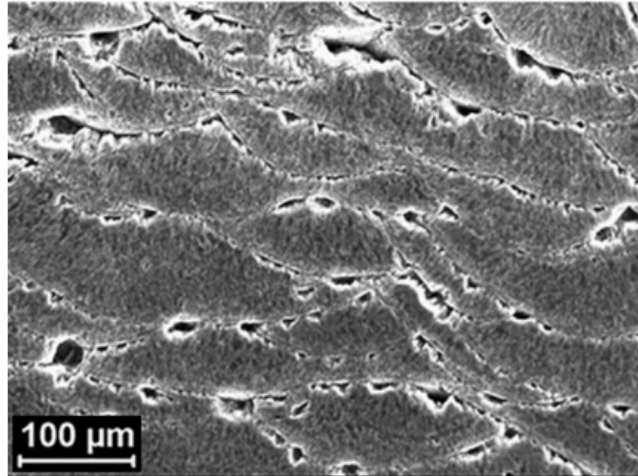

Figure 1. (**a**) Secondary electron image representing the microstructure of additively manufactured Al-Si alloys (AlSi10Mg). The surface parallel to the building platform is represented here. Similar features can be observed in the surface perpendicular to the building platform, but the shape of the cells is more elongated in that case. (**b**) Higher magnification image of a zone in the melt pool border. (**c**) Higher magnification image of a zone within the melt pool. MPB —melt pool border; HAZ—heat-affected zone. (Adapted from reference [32]).

A great number of works have already shown that the corrosion behaviour of additively manufactured Al-Si alloys is greatly influenced by this special and unique microstructure created during the additive manufacturing process.
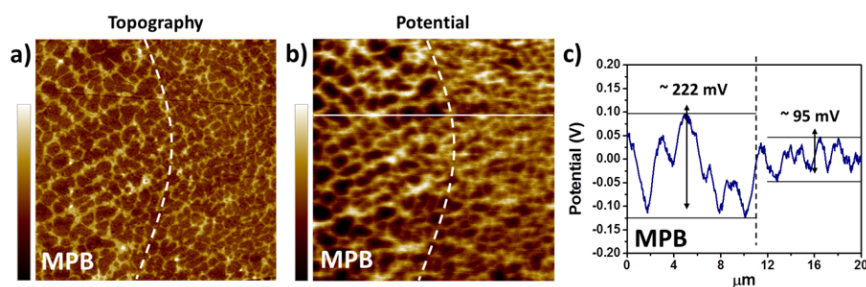
2.1.1. Influence of the Melt Pool Borders on Corrosion

Among the different details of the microstructural features of as-built AM Al-Si alloys, the borders of the melt pools have been pointed out to be a key element in the corrosion of these materials. Several studies have shown that after potentiodynamic polarization tests and/or immersion in NaCl solution a particularly pronounced selective corrosion of the α-Al cells in the melt pool borders is observed (see Figure 2) [33][34][35][36][37][38][39][40][41][42][43][44][45][46][47][48]. This selective corrosion attack along the borders of the melt pools has been reported for polished and ground specimens [33][34][35][36][37][38][39][40][41][42][43][44][45][46][47], but also for as-built materials presenting a low surface roughness [48], for which the microstructural features are believed to control the electrochemical performance of the material.

Figure 2. Secondary electron microscopy image of the surface of an as-built AM Al-Si (AlSi10Mg) corroded in NaCl solution. (Adapted from reference [38]).

The initiation and further propagation of the corrosion attack in the Al cells along the MPBs are caused by the higher driving force for micro-galvanic corrosion between the α-Al and the Si phase in these regions compared to other areas within the melt pools [33][36][45]. Due to the presence of a relatively larger microstructure at the MPBs (see Figure 3), a greater Volta-potential difference has been reported between the Al and the Si phase compared to regions within the MPs (Figure 3c). Nevertheless, Kubacki et al. [42] do not support the assumption of a galvanic couple between the Al and Si phase accelerating corrosion in simulated atmospheric conditions at the melt pool borders. The researchers believe that under these conditions the cathodic kinetics on the Si phase is not fast enough to support the active dissolution of Al. Instead, the selective/pronounced corrosion attack at the borders of the melt pools is attributed to the high discontinuities of the Si network around the MPBs (in the heat-affected zone).
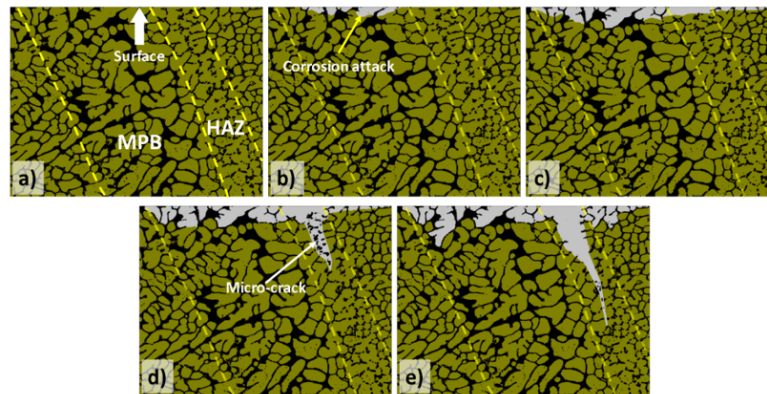

Figure 3. (**a**) Topography and (**b**) surface potential map (obtained by scanning Kelvin probe force microscopy – SKPFM) of an area on the surface of a polished AM AlSi10Mg specimen in which a melt pool border is visible (delimited by the discontinuous line). Scan size: 20 × 20 μm^2. Colour bar: (**a**) 30 nm range, (**b**) 210 mV range. (**c**) Surface potential profile of the line represented in (**b**). (Adapted from reference [33]).

The morphology of the corrosion attack in as-built AM Al-Si alloys has been described by several researchers to be rather superficial due to the existence of a considerably connected Si network that holds the corrosion from penetrating deeper into the material [33][34][42][45][49]. However, several works have found a large penetration of the corrosion attack along the melt pool borders [37][41][42][43][44][46]. Moreover, the formation of micro-cracks during corrosion has been reported in regions next to the MPBs, where heat-affected zones exist [33][34][45][46][50]. As mentioned above, Revilla et al. [34] associated the formation of these micro-cracks to the synergistic effect of the selective dissolution of the α-Al cells along

the MPBs, next to which the disrupted heat-affected zones are found, and the existence of internal and superficial residual stresses from the MAM process. Rafiezad et al. [40] also confirmed through intergranular corrosion test an accelerated preferential attack combined with the formation of micro-cracks along the melt pool borders for specimens fabricated using recycled powder. Moreover, while conducting electrochemical tests in NaCl solution, Girelli et al. [50] found that the MPBs/HAZ represent preferential paths for exfoliation-like corrosion to occur.

The schematic in Figure 4 shows the proposed evolution of the corrosion attack in as-built AM Al-Si alloys [34]. Because of the greater Volta-potential difference between the α-Al and the Si phase at the melt pool borders (as measured by scanning Kelvin probe force microscopy SKPFM [33][36][45]—see Figure 3), a higher driving force for galvanic corrosion provokes the initiation of the corrosion attack in these regions. The corrosion spreads superficially to adjacent zones, including the neighbouring heat-affected zones. This corrosion is partially contained by the connected portion of the Si network. However, due to the disruption in the heat-affected zone, the corrosion can propagate further into the material along the MPBs.

Figure 4. Schematic diagram representing the process of corrosion initiation and corrosion propagation for as-built additively manufactured Al-Si alloys. The illustrations portray the corrosion process seen from a cross-sectional perspective, with the top side of the images representing the surface exposed to the corrosive medium. The Al phase is represented with green, while black portrays the Si phase. A melt pool border (MPB), where a coarser microstructure is seen, and a heat-affected zone (HAZ), characterized by discontinuities in the Si network, can be observed in the images (**a**). The corrosion attack initiates at the MPB, where there is a larger potential difference between the Al and the Si phase, and therefore, a larger driving force for galvanic corrosion (**b**). Because of the partial containment of the corrosion by the Si network, the attack spreads superficially to adjacent zones, reaching the HAZ (**c**). Due to the disruption of the Si network in the HAZ, combined with the existence of internal stresses from the MAM process, micro-cracks are formed along the HAZ (**d**). In a later stage of the corrosion, additional lateral spreading of the attack occurs, accompanied by further propagation of the crack and corrosive medium through the HAZ (**e**) [34].
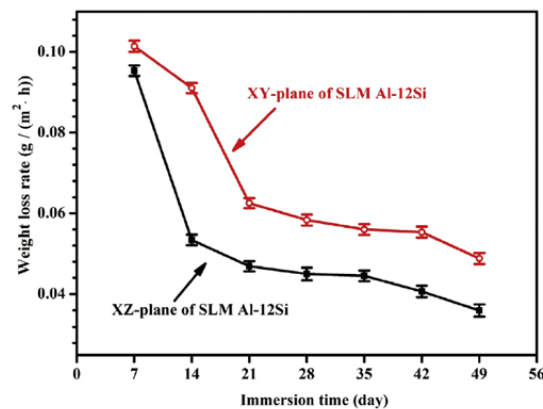
2.1.2. Anisotropy

As already mentioned, the special microstructure of additively manufactured Al-Si alloys is the result of the exceptionally high cooling rates and direction of the thermal gradients . The particular directional distribution of thermal gradients during the fusion and solidification of the different layers of the material produces an intrinsically anisotropic microstructure [25]. The small α-Al cells surrounded by the Si network are rather rounded in the plane parallel to the building platform, while in the plane perpendicular to the building platform these cells have an elongated shape [25]. Additionally, in the surfaces parallel to the building platform (XY plane), elongated laser tracks are easily identified, while in the surfaces perpendicular to the building platform (XZ plane) a scale-like feature of melt pool borders is generally seen [33][34][35][36][37][38][39].

Concerning the influence of this anisotropy on the corrosion behaviour/resistance of these materials, various and contradictory results have been reported in the literature. For AlSi10Mg prepared by SLM, Cabrini et al. [39][41] concluded from potentiodynamic polarization experiments in diluted Harrison's solution that the surface of the XZ plane presents a slightly lower pitting corrosion resistance than the XY plane. The researchers associated this behaviour with the higher density of melt pool borders found in the XZ plane compared to that of the XY plane. However, in a later work, the same researchers concluded through a statistical approach that the building direction does not significantly influence the corrosion resistance of the analysed surface [47]. Moreover, Revilla et al. [33][34][45] found no difference in the electrochemical behaviour of the different planes during potentiodynamic polarization tests in aerated NaCl solution.

On the other hand, Cabrini et al. [37] demonstrated in another work by conducting an intergranular corrosion test that the corrosion in as-built specimens propagates mainly along the MPBs. Therefore, the penetration depth of the corrosion attack is highly influenced by the anisotropy of the melt pools. A more penetrative corrosion attack was seen on the

surface parallel to the building platform compared to the surface perpendicular to the building platform. This could demonstrate that even if similar electrochemical behaviour is seen during potentiodynamic polarization tests, great anisotropy can still exist on the morphology of the corrosion attack and corrosion penetration depth.

For SLM AlSi7Mg0.6 and AlSi12, no considerable difference was reported between the behaviours of the two different planes during potentiodynamic polarization tests in NaCl solution [34]. Nevertheless, a clear distinction in the corrosion resistance of the different planes was shown by Chen et al. [31] for SLM Al-Si12. The researchers presented experimental data (open circuit potential, potentiodynamic polarization, and electrochemical impedance spectroscopy measurements) supporting a better corrosion resistance of the XZ plane compared to the XY plane. This is the opposite trend as that reported for AlSi10Mg by Cabrini et al. [39][41]. Chen et al. [31] associated this behaviour with the depth of the Al/Si cells in each plane. The small and round cells were seen in the XY plane are deep since they are elongated in the perpendicular direction. According to the researchers, this could lead to the growth and even deposition of corrosion products, which could extrude and crack the Si shells, exposing the underlying Al substrate to further corrosion attack. On the other hand, the cells seen in the XZ plane are shallow, which could limit/prevent the deposition of corrosion products. Moreover, Chen et al. [31] reported a clear difference in the weight loss rate during corrosion in NaCl solution for the different planes. These results are shown in Figure 5. A reduced weight loss rate is seen for the XZ plane compared to the XY plane, possibly due to the same reason as that given for the difference in the electrochemical behaviour.

Figure 5. The weight loss rate for the different surface planes (parallel to the building platform—XY—and perpendicular to the building platform—XZ) of as-built and mechanically polished SLM AlSi12 after immersion in 3.5 wt.% NaCl solution at room temperature [31].

Due to the limited and contradictory results found in literature concerning the effect of the anisotropic microstructure on the corrosion behaviour, further research is needed to better understand this issue. It is also important to keep in mind that different alloys (even from the same alloy family) might display intrinsically different behaviours.

References

1. Murr, L.E.; Gaytan, S.M.; Ramirez, D.A.; Martinez, E.; Hernandez, J.; Amato, K.N.; Shindo, P.W.; Medina, F.R.; Wicker, R.B. Metal Fabrication by Additive Manufacturing Using Laser and Electron Beam Melting Technologies. Mater. Sci. Technol. 2012, 28, 1–14, doi:10.1016/s1005-0302(12)60016-4.

2. Murr, L.; Martinez, E.; Amato, K.N.; Gaytan, S.M.; Hernandez, J.; Ramirez, D.A.; Shindo, P.W.; Medina, F.; Wicker, R.B. Fabrication of Metal and Alloy Components by Additive Manufacturing: Examples of 3D Materials Science. Mater. Res. Technol. 2012, 1, 42–54, doi:10.1016/s2238-7854(12)70009-1.

3. Herzog, D.; Seyda, V.; Wycisk, E.; Emmelmann, C. Additive manufacturing of metals. Acta Mater. 2016, 117, 371–392.

4. Sames, W.J.; List, F.A.; Pannala, S.; Dehoff, R.R.; Babu, S.S. The metallurgy and processing science of metal additive manufacturing. Mater. Rev. 2016, 61, 315–360, doi:10.1080/09506608.2015.1116649.

5. Gorsse, S.; Hutchinson, C.; Goune, M.; Banerjee, R. Additive manufacturing of metals: A brief review of the characteristic microstructures and properties of steels, Ti-6Al-4V and high-entropy alloys. Sci. Technol. Adv. Mater. 2017, 18, 584–610.

6. Gu, D.; Meiners, W.; Wissenbach, K.; Poprawe, R. Laser additive manufacturing of metallic components: Materials, processes and mechanisms. Mater. Rev. 2012, 57, 133–164, doi:10.1179/1743280411y.0000000014.

7. ISO/ASTM52900-15. Standard Terminology for Additive Manufacturing—General Principles—Terminology; ASTM International: West Conshohocken, PA, USA, 2015.

8. Sun, G.; Shen, X.; Wang, Z.; Zhan, M.; Yao, S.; Zhou, R.; Ni, Z. Laser metal deposition as repair technology for 316L stainless steel: Influence of feeding powder compositions on microstructure and mechanical properties. Laser Technol. 2019, 109, 71–83, doi:10.1016/j.optlastec.2018.07.051.

9. Dilberoglu, U.M.; Gharehpapagh, B.; Yaman, U.; Dolen, M. The Role of Additive Manufacturing in the Era of Industry 4.0. Procedia Manuf. 2017, 11, 545–554, doi:10.1016/j.promfg.2017.07.148.

10. Additive Manufacturing Report. Available online: https://additive-manufacturing-report.com/additive-manufacturing-market/ (accessed on October 16, 2020).

11. DebRoy, T.; Wei, H.L.; Zuback, J.S.; Mukherjee, T.; Elmer, J.W.; Milewski, J.O.; Beese, A.M.; Wilson-Heid, A.; De, A.; Zhang, W. Additive manufacturing of metallic components—Process, structure and properties. Mater. Sci. 2018, 92, 112–224.

12. Additive Manufacturing for the Aerospace Industry; Elsevier: Amsterdam, The Netherlands, 2019.

13. Miller, W.; Zhuang, L.; Bottema, J.; Wittebrood, A.; De Smet, P.; Haszler, A.; Vieregge, A. Recent development in aluminium alloys for the automotive industry. Sci. Eng. A 2000, 280, 37–49, doi:10.1016/s0921-5093(99)00653-x.

14. Available Materials for Metal Additive Manufacturing: Characteristics & Applications, Farinia Group. Available online: https://www.farinia.com/additive-manufacturing/3dmaterials/characteristics-and-applications-ofavailable-metals-for-additive-manufacturing (accessed on September 7, 2020).

15. Aboulkhair, N.T.; Simonelli, M.; Parry, L.; Ashcroft, I.; Tuck, C.; Hague, R. 3D printing of Aluminium alloys: Additive Manufacturing of Aluminium alloys using selective laser melting. Mater. Sci. 2019, 106, 100578, doi:10.1016/j.pmatsci.2019.100578.

16. Vojtech, D.; Serak, J.; Ekrt, O. Improving the casting properties of high-strength aluminium alloys. Mater. Technol. 2004, 38, 99–102.

17. Zhang, J.; Song, B.; Wei, Q.; Bourell, D.; Shi, Y. A review of selective laser melting of aluminum alloys: Processing, microstructure, property and developing trends. Mater. Sci. Technol. 2019, 35, 270–284, doi:10.1016/j.jmst.2018.09.004.

18. ASM Handbook; ASM International: Materials Park, OH, USA, 1991; Volume 4.

19. Sander, G.; Tan, J.; Balan, P.; Gharbi, O.; Feenstra, D.; Singer, L.; Thomas, S.; Kelly, R.; Scully, J.; Birbilis, N. Corrosion of Additively Manufactured Alloys: A Review. Corrosion 2018, 74, 1318–1350, doi:10.5006/2926.

20. Kong, D.; Dong, C.; Ni, X.; Li, X. Corrosion of metallic materials fabricated by selective laser melting. NPJ Mater. Degrad. 2019, 3, 24, doi:10.1038/s41529-019-0086-1.

21. Chen, H.; Zhang, C.; Jia, D.; Wellmann, D.; Liu, W. Corrosion Behaviors of Selective Laser Melted Aluminum Alloys: A Review. Metals 2020, 10, 102, doi:10.3390/met10010102.

22. Revilla, R.I.; De Graeve, I. Influence of Si content on the microstructure and corrosion behaviour of additive manufactured Al-Si alloys. Electrochem. Soc. 2018, 165, C926–C932.

23. Brandl, E.; Heckenberger, U.; Holzinger, V.; Buchbinder, D. Additive manufactured AlSi10Mg samples using Selective Laser Melting (SLM): Microstructure, high cycle fatigue, and fracture behavior. Des. 2012, 34, 159–169, doi:10.1016/j.matdes.2011.07.067.

24. Manfredi, D.; Calignano, F.; Krishnan, M.; Canali, R.; Ambrosio, E.P.; Atzeni, E. From Powders to Dense Metal Parts: Characterization of a Commercial AlSiMg Alloy Processed through Direct Metal Laser Sintering. Materials 2013, 6, 856–869, doi:10.3390/ma6030856.

25. Thijs, L.; Kempen, K.; Kruth, J.-P.; Van Humbeeck, J. Fine-structured aluminium products with controllable texture by selective laser melting of pre-alloyed AlSi10Mg powder. Acta Mater. 2013, 61, 1809–1819, doi:10.1016/j.actamat.2012.11.052.

26. Yan, C.; Hao, L.; Hussein, A.; Young, P.; Huang, J.; Zhu, W. Microstructure and mechanical properties of aluminium alloy cellular lattice structures manufactured by direct metal laser sintering. Sci. Eng. A 2015, 628, 238–246, doi:10.1016/j.msea.2015.01.063.

27. Li, W.; Li, S.; Liu, J.; Zhang, A.; Zhou, Y.; Wei, Q.; Yan, C.; Shi, Y. Effect of heat treatment on AlSi10Mg alloy fabricated by selective laser melting: Microstructure evolution, mechanical properties and fracture mechanism. Sci. Eng. A 2016, 663, 116–125, doi:10.1016/j.msea.2016.03.088.

28. Prashanth, K.; Scudino, S.; Klauss, H.; Surreddi, K.; Löber, L.; Wang, Z.; Chaubey, A.; Kühn, U.; Eckert, J. Microstructure and mechanical properties of Al–12Si produced by selective laser melting: Effect of heat treatment. Sci. Eng. A 2014, 590, 153–160, doi:10.1016/j.msea.2013.10.023.

29. Kimura, T.; Nakamoto, T.; Mizuno, M.; Araki, H. Effect of silicon content on densification, mechanical and thermal properties of Al-xSi binary alloys fabricated using selective laser melting. Sci. Eng. A 2017, 682, 593–602, doi:10.1016/j.mse

a.2016.11.059.

30. Revilla, R.I.; Verkens, D.; Couturiaux, G.; Malet, L.; Thijs, L.; Godet, S.; De Graeve, I. Galvanostatic Anodizing of Additive Manufactured Al-Si10-Mg Alloy. Electrochem. Soc. 2017, 164, C1027–C1034, doi:10.1149/2.1121714jes.

31. Chen, Y.; Zhang, J.; Gu, X.; Dai, N.; Qin, P.; Zhang, L.-C. Distinction of corrosion resistance of selective laser melted Al-12Si alloy on different planes. Alloys Compd. 2018, 747, 648–658, doi:10.1016/j.jallcom.2018.03.062.

32. Revilla, R.I.; Terryn, H.; De Graeve, I. Role of Si in the Anodizing Behavior of Al-Si Alloys: Additive Manufactured and Cast Al-Si10-Mg. J. Electrochem. Soc. 2018, 165, C532–C541.

33. Revilla, R.I.; Liang, J.; Godet, S.; De Graeve, I. Local Corrosion Behavior of Additive Manufactured AlSiMg Alloy Assessed by SEM and SKPFM. J. Electrochem. Soc. 2016, 164, C27–C35.

34. Revilla, R.I.; De Graeve, I. Influence of Si content on the microstructure and corrosion behaviour of additive manufactured Al-Si alloys. J. Electrochem. Soc. 2018, 165, C926–C932.

35. Fathi, P.; Mohammadi, M.; Duan, X.; Nasiri, A. A comparative study on corrosion and microstructure of direct metal laser sintered AlSi10Mg_200C and die cast A360.1 aluminum. J. Mater. Process. Technol. 2018, 259, 1–14.

36. Cabrini, M.; Lorenzi, S.; Pastore, T.; Testa, C.; Manfredi, D.; Lorusso, M.; Calignano, F.; Pavese, M.; Andreatta, F. Corrosion behavior of AlSi10Mg alloy produced by laser powder bed fusion under chloride exposure. Corros. Sci. 2019, 152, 101–108.

37. Cabrini, M.; Lorenzi, S.; Pastore, T. Corrosion behavior of aluminum-silicon alloys obtained by Direct Metal Laser Sintering. In Proceedings of the EUROCORR 2017—The Annual Congress of the European Federation of Corrosion, 20th International Corrosion Congress and Process Safety Congress 2017, Prague, Czech Republic, 3–7 September 2017.

38. Cabrini, M.; Lorenzi, S.; Pastore, T.; Testa, C.; Manfredi, D.; Cattano, G.; Calignano, F. Corrosion resistance in chloride solution of the AlSi10Mg alloy obtained by means of LPBF. Surf. Interface Anal. 2018, 51, 1159–1164.

39. Cabrini, M.; Lorenzi, S.; Pastore, T.; Pellegrini, S.; Pavese, M.; Fino, P.; Ambrosio, E.P.; Calignano, F.; Manfredi, D. Corrosion resistance of direct metal laser sintering AlSiMg alloy. Surf. Interface Anal. 2016, 48, 818–826.

40. Rafieazad, M.; Chatterjee, A.; Nasiri, A.M. Effects of Recycled Powder on Solidification Defects, Microstructure, and Corrosion Properties of DMLS Fabricated AlSi10Mg. JOM 2019, 71, 3241–3252.

41. Cabrini, M.; Lorenzi, S.; Pastore, T.; Pellegrini, S.; Manfredi, D.G.; Fino, P.; Biamino, S.; Badini, C.F. Evaluation of corrosion resistance of Al–10Si–Mg alloy obtained by means of Direct Metal Laser Sintering. J. Mater. Process. Technol. 2016, 231, 326–335.

42. Kubacki, G.; Brownhill, J.P.; Kelly, R.G. Comparison of Atmospheric Corrosion of Additively Manufactured and Cast Al-10Si-Mg over a Range of Heat Treatments. Corrosion 2019, 75, 1527–1540.

43. Cabrini, M.; Calignano, F.; Fino, P.; Lorenzi, S.; Lorusso, M.; Manfredi, D.; Testa, C.; Pastore, T. Corrosion Behavior of Heat-Treated AlSi10Mg Manufactured by Laser Powder Bed Fusion. Materials 2018, 11, 1051.

44. Cabrini, M.; Lorenzi, S.; Pastore, T.; Pellegrini, S.; Ambrosio, E.P.; Calignano, F.; Manfredi, D.G.; Pavese, M.; Fino, P. Effect of heat treatment on corrosion resistance of DMLS AlSi10Mg alloy. Electrochim. Acta 2016, 206, 346–355.

45. Rubben, T.; Revilla, R.I.; De Graeve, I. Influence of heat treatments on the corrosion mechanism of additive manufactured AlSi10Mg. Corros. Sci. 2019, 147, 406–415.

46. Rafieazad, M.; Mohammadi, M.; Nasiri, A. On microstructure and early stage corrosion performance of heat treated direct metal laser sintered AlSi10Mg. Addit. Manuf. 2019, 28, 107–119.

47. Cabrini, M.; Lorenzi, S.; Testa, C.; Pastore, T.; Manfredi, D.; Lorusso, M.; Calignano, F.; Fino, P. Statistical approach for electrochemical evaluation of the effect of heat treatments on the corrosion resistance of AlSi10Mg alloy by laser powder bed fusion. Electrochim. Acta 2019, 305, 459–466.

48. Fathi, P.; Rafieazad, M.; Duan, X.; Mohammadi, M.; Nasiri, A. On microstructure and corrosion behaviour of AlSi10Mg alloy with low surface roughness fabricated by direct metal laser sintering. Corros. Sci. 2019, 157, 126–145.

49. Gu, X.-H.; Zhang, J.-X.; Fan, X.-L.; Zhang, L.-C. Corrosion Behavior of Selective Laser Melted AlSi10Mg Alloy in NaCl Solution and Its Dependence on Heat Treatment. Acta Met. Sin. 2019, 33, 327–337.

50. Girelli, L.; Tocci, M.; Conte, M.; Giovanardi, R.; Veronesi, P.; Gelfi, M.; Pola, A. Effect of the T6 heat treatment on corrosion behavior of additive manufactured and gravity cast AlSi10Mg alloy. Mater. Corros. 2019, 70, 1808–1816.